Journal of Power Sources 218 (2012) 424–434

Contents lists available at SciVerse ScienceDirect

Journal of Power Sources

journal homepage: www.elsevier.com/locate/jpowsour

Comparison of Pt and Pd catalysts for hydrogen pump separation from reformate

Xuemei Wu [a], Jay Benziger [b,*], Gaohong He [a]

[a] State Key Laboratory of Fine Chemicals, Research and Development Center of Membrane Science and Technology, Dalian University of Technology, Dalian 116024, PR China
[b] Department of Chemical and Biological Engineering, Princeton University, Princeton, NJ 08540, USA

HIGHLIGHTS

- H_2 was purified with a PEM hydrogen pump with Pd/C catalysts.
- Pd/C catalysts were less efficient than Pt/C catalysts for H_2 purification.
- CO_2 adsorbs on Pd catalysts reducing the electroactive surface area.
- The effective MEA resistance increases with decreases in H_2 partial pressure.
- Gas phase diffusion contributes to the effective MEA resistance.

ARTICLE INFO

Article history:
Received 4 May 2012
Received in revised form
28 June 2012
Accepted 1 July 2012
Available online 6 July 2012

Keywords:
Hydrogen purification
Electrochemical separations
Electrocatalyst coated membranes

ABSTRACT

Hydrogen recovery from CO_2/H_2 reformate mixtures by selective electrochemical pumping was compared from carbon supported Pt and Pd catalysts. Catalyst coated membranes were prepared by air-brushing a suspension of commercially available 20 wt% Pt/C or 20 wt% Pd/C catalysts and solubilized Nafion in methanol onto Nafion 115 membranes. Electrochemical activity and separation efficiency for the different catalyst layer formulations were evaluated by cyclic voltammetry, polarization and potentiostatic hydrogen pumping. The effective membrane-electrode-assembly (MEA) resistance increased due to dilution of H_2 by CO_2; the effective MEA resistance was greater for Pd/C catalysts than for Pt/C catalysts. CO_2 adsorbed more strongly to Pd catalysts than Pt catalysts reducing the electrochemical active surface area available for hydrogen oxidation/reduction. Pd/C catalysts had an energy efficiency for hydrogen recovery from reformate mixtures approximately 80% that of Pt catalysts. Because Pd is ten times less costly than Pt the results presented here suggest that Pd/C catalysts would be a promising candidate for hydrogen pumps to recover H_2 from reformate mixtures.

1. Introduction

Hydrogen is an attractive alternative to fossil fuel. It does not produce any pollutants at its point of use. Hydrogen can be produced by steam reforming coal, petroleum or natural gas. Steam reforming coupled with the water gas shift reaction produces a reformate mixture of CO_2, H_2, H_2O [1,2]. Hydrogen can then be separated from the reformate mixture. The CO_2 can be sequestered while the H_2 can be used in fuel cells, gas turbines or even internal combustion engines. To reduce greenhouse gas emissions, it is important to develop technologies that integrate hydrogen recovery and CO_2 capture [3,4]. There are several well established technologies to separate H_2 and CO_2. Alkaline/amine scrubbing is employed for large scale hydrogen purification by the ammonia synthesis industry [5–7]. For smaller applications requiring higher purity hydrogen, pressure swing adsorption (PSA) has been employed [8–11]. Both scrubbing and PSA processes focus on CO_2 capture rather than H_2 purification. The net energy efficiency for hydrogen recovery is ~80% for amine scrubbing and ~70–75% for PSA. The overall energy efficiency of these processes for hydrogen purification is reduced by additional steps to purify the H_2 product if high purity H_2 is required for fuel cell applications.

The polymer electrolyte hydrogen pump (PEHP) is a promising alternative to efficiently recover hydrogen from reformate mixtures. A proton conducting polymer (e.g. Nafion) is sandwiched between two catalytic electrodes. When an external potential is applied across the electrodes, hydrogen is oxidized by the anode catalyst to protons, the protons are transported across the polymer electrolyte membrane and subsequently reduced by the cathode catalyst to hydrogen again. Only hydrogen is pumped through the polymer membrane producing a very pure hydrogen product

* Corresponding author. Tel.: +1 609 258 5416; fax: +1 609 258 0211.
E-mail address: benziger@princeton.edu (J. Benziger).

0378-7753/$ – see front matter © 2012 Elsevier B.V. All rights reserved.
http://dx.doi.org/10.1016/j.jpowsour.2012.07.002

(>99.7% purity) [12,13]. At the same time the hydrogen is recovered, the CO_2 is concentrated and could be captured from the effluent of the anode without further treatment. The trace impurities which are left in the CO_2 do not pose a problem for sequestration. Another advantage of hydrogen pumping is that with a modest increase of the applied potential, the hydrogen product can be compressed up to 100 bars in a single stage [14–17]. The hydrogen from the PEHP could be employed as fuel or as reactant for hydrogenation reactions [18–21].

The PEHP can be traced back to the 1980s [22]. Several investigators have studied hydrogen recovery from hydrogen-rich fuel streams (H_2/N_2, $H_2/CO_2/CO$, H_2/CH_4, etc.) [12,13,23–25] or waste gases (the anode effluent from fuel cells or the product stream from hydrocarbon reforming) [26,27]. Most of the studies focused on the issues of current efficiency and the effects of impurities [28,29]. Benziger et al. examined the net energy efficiency as a function of hydrogen recovery from H_2/CO_2 streams. They showed that single stage hydrogen pumps have a maximum energy efficiency of 70%, but the net energy efficiency can be increased to >90% with 99% recovery with a multi-stage H_2/CO_2 PEHP separator [12]. The multistage PEHP design of Benziger et al. showed net energy efficiencies for H_2 purification from H_2/CO_2 reformate mixtures that exceeded amine scrubbing. The two major barriers to commercial development of the PEHP purification process are to reduce the cost of the catalysts employed and to deal with catalyst poisoning by impurities in the reformate stream. Gardner and Benicewicz examined operational conditions to improve tolerance to carbon monoxide and sulfur impurities in reformate [30,31]. They showed that periodic voltage pulsing and increased operating temperature improved hydrogen yields in the presence of impurities.

All the previous studies used platinum as the catalyst. For large scale application of PEHPs the cost of Pt catalysts could result in excessive capital investment costs, which are crucial in assessing the commercial viability of the PEHP compared to other commercial hydrogen separation techniques.

In the present study, we investigate the possibility of replacing Pt with Pd as the catalyst for the reformate separation in PEHP. Pd is fifty times more abundant on the earth than Pt, so the price of Pd is substantially lower than that of Pt. Pd-based catalysts have been tested as alternatives to Pt in fuel cell application. In the presence of pure hydrogen or reformate, Pd exhibited "acceptable" electrochemical activity for the hydrogen oxidation reaction (HOR) [32,33]. Pd and Pt/Pd alloy catalysts had reduced HOR compared to Pt, but the rates were sufficiently large so the activation polarization loss was not significant. Addition of a small amount (5%) of Pt to Pd produced catalysts with comparable HOR activity to that of pure Pt, and the resistance to CO contamination was higher for the Pd/Pt alloy [34,35]. However, we did not encounter any studies of the difference between Pt and Pd for both the hydrogen oxidation and proton reduction reactions which are the basis of the hydrogen pump.

The present study compares PEHP performance for separating H_2/CO_2 mixtures with Pd and Pt catalysts. Electrochemical activity of Pd/C and Pt/C catalysts was investigated by potentiostatic studies, cyclic voltammetry and polarization studies at different CO_2/H_2 ratios. We also studied the effects of catalyst loading, and Nafion loading in the catalyst layer. The results show that membrane-electrode-assemblies made with commercial Pd/C catalysts have a larger effective resistance than Pt/C catalysts. This was shown to result from (1) less efficient dispersion of Pd than Pt on the carbon support, and (2) catalyst poisoning from reversible CO_2 adsorption on Pd catalysts. H_2 dilution by CO_2 was shown to result in mass transport resistances which limited the recovery of H_2. A modified transport model that balances diffusion of H_2 in the catalysts pores, H_2 diffusion across a thin Nafion film covering the active catalyst and proton transport through the Nafion film in the catalyst layer is presented to account for the performance differences of PEHP with Pt/C and Pd/C catalysts.

2. Experimental

2.1. Preparation of the membrane electrode assemblies (MEAs)

The membrane electrode assemblies for the PEHP consisted of catalyst coated Nafion membranes sandwiched between gas diffusion electrodes. Most studies employed gas diffusion electrodes (GDEs) consisting of carbon paper with a micro-porous layer (MPL) on one side (GDL 35BC by SGL Tech., Germany). Nafion 115 membranes (Ion Power Inc., New Castle, DE) were pretreated by sequential boiling for 1 h in 3 wt% hydrogen peroxide, deionized water, 1 M sulfuric acid and deionized water. The catalyst coating was prepared by air-brushing a suspension of 20 wt% Pt/C or 20 wt% Pd/C catalysts (Premetek Co. Wilmington, DE) and solubilized Nafion in methanol. The carbon support was Vulcan XC-72; nominal particle sizes and BET surface areas provided by Premetek are listed in Table 1. The catalyst loading (M_{cat}) was adjusted to give values of 0.5 mg Pt cm^{-2} or 0.4–0.8 mg Pd cm^{-2}. The Nafion loading (w_N) in the catalyst layer was adjusted by varying the concentration ratio in the solution employed for air-brushing. The catalyst coated membrane was sandwiched between two GDEs with the microporous layers contacting the catalyst layers. The MEA was clamped between two stainless steel plates and sealed in around the edges with a silicon rubber gasket.

2.2. Performance of PEHP

The PEHP used in this study was based on the one-dimensional differential or stirred tank reactor (STR) fuel cell design developed by Benziger and co-workers [36,37]. The MEA was clamped between two graphite plates with machined channel-less, self-draining flow fields. The flow field design provides a uniform gas composition and allows liquid water to drain by gravity. The MEA in the PEHP had a nominal electrode/electrolyte area of 1.9 cm^2.

The setup of the PEHP separator is shown schematically in Fig. 1. Hydrogen and carbon dioxide were metered through mass flow controllers, mixed, bubbled through water in a humidifier and fed to the anode. The humidifier temperature was 15 °C higher than the PEHP temperature to provide water saturated feed gas. The cathode inlet was sealed. The effluents from the anode and cathode were bubbled through liquid water reservoirs to block back flow of air. The operating pressures at the anode and cathode were ~1 kPa above atmospheric pressure. Gas flow rates exiting both the anode and cathode were measured by water displacement, confirming that the hydrogen mass balance closed to within 5%.

Electrochemical hydrogen pumping was evaluated by measuring the current/voltage response functions. An Arbin potentiostat/galvanostat MSTAT4+ test station was used to create programmed schedules of current or applied potential and measure voltage or current response respectively. The current–voltage

Table 1
Properties of the Pt/C and Pd/C catalysts.

	Pt/C	Pd/C
Weight loading (wt%)	20	20
BET surface area ($m^2\ g^{-1}$)	~250	~250
Active surface area ($m^2\ g^{-1}$)	20	28
Carbon particle size (nm)	30	30
Metal particle size (nm)	2.5 ± 0.3	3.5 ± 0.5
Metal surface density (mmol g^{-1})	1.28	2.36

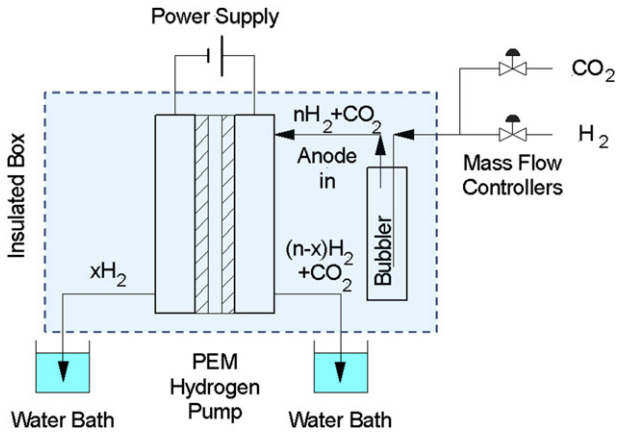

Fig. 1. Schematic of the PEHP experimental setup.

polarization curve was obtained with both voltage and current ramps; only the polarization curves from voltage ramps are reported here. The current through the cell was measured in response to a voltage ramp from 0 to 0.04 V at 0.05 mV s^{-1}.

The H_2 separation efficiency was evaluated by measuring the current response to a series of voltage steps and hold. The applied potential was stepped from 0.04 to 0.32 V by increments of 0.04 V, and then stepped to 0.4, 0.5 and 0.55 V. The potential was held for 1 h at each voltage. The internal resistance of the MEA was measured by pulsed current relaxation every 30 min. Tests were carried out with fully humidified feeds. The dry feed flow rate was 16 sccm with CO_2/H_2 (C/H) and N_2/H_2 ratios of 0, 1/4, 1/3, 1/2, 1/1 and 2/1. Tests were run at 30 and 50 °C. All experiments were conducted at constant flow rate so that flow control dynamics were decoupled from reactor dynamics.

2.3. Electrochemical characterization

Cyclic voltammetry (CV) was performed at 30 °C in-situ in the two-electrode PEHP utilizing the Arbin potentiostat/galvanostat [38]. The Pt/C cathode was fed with 50 ml min^{-1} humidified hydrogen; it acted as both reference and counter electrodes. Pt/C or Pd/C anodes fed with 50 ml min^{-1} humidified nitrogen acted as the working electrode. CO_2 adsorbate stripping CV was carried out using the procedure reported in the literature by de Bruijn et al. [39]. The working electrode was exposed to humidified CO_2/H_2 mixtures and operated in the PEHP mode at 0.2 V for 1 h. The applied potential was then set to 0 V and the working electrode was flushed with humidified nitrogen for 30 min in order to remove all the CO_2 in the gas phase in the cathode compartment. The current was then measured as the potential was scanned from 0 to 1.2 V_{RHE} at a scan rate of 20 mV s^{-1}.

3. Results

3.1. Toward an optimal catalyst layer

Previous work with the polymer electrolyte hydrogen pump employed a standard catalyst layer composition: 0.5 mg Pt cm^{-2} of 20 wt% Pt supported on Vulcan carbon with 1.42 (g-Nafion)(g-Pt)$^{-1}$. For our comparison study we obtained 20 wt% Pt and 20 wt% Pd supported on Vulcan carbon from Premetek. Because of different densities of Pt and Pd the electrocatalytic active surface areas were different even though they had the same mass loading. A series of experiments were carried out to identify the optimal catalyst layer composition for a 20 wt% Pd/C catalyst.

Table 2
Pd/C catalyst layer screening.

Catalyst loading (mg-Pd cm^{-2})	0.27, 0.4, 0.5, 0.6, 0.7	0.4	0.4
Nafion loading (g-Nafion)(g-Pd)$^{-1}$	1.42	0.88, 1.42, 2.14, 3.33	1.42
GDL material	Carbon paper with MPL	Carbon paper with MPL	Carbon cloth with MPL

Membrane electrode assemblies were prepared with identical Pt/C anodes (0.5 mg-Pt cm^{-2}) and Pd/C cathode catalyst layers with varying Pd loading, Nafion loading, and different GDL materials as summarized in Table 2.

Current was measured as a function of applied potential at 50 °C for MEAs with cathode compositions listed in Table 2; the results for different catalyst loadings and different Nafion loadings are shown in Figs. 2 and 3. A baseline experiment done with the standard Pt/C catalyst is shown in Fig. 2 for comparison.

The optimal MEA was judged to be where the MEA has the lowest effective resistance (i.e. the slope of the *IV* curve is maximum). The best performing Pd MEAs had Pd loading of 0.4–0.5 mg cm^{-2}, with 1.42 (g-Nafion)(g-Pd)$^{-1}$ and a carbon paper GDL. All the experiments for hydrogen separation from H_2/CO_2 mixtures were performed with this MEA composition.

3.2. Performances of hydrogen pump with Pt/C and Pd/C catalysts

Typical results for hydrogen separation from a H_2/CO_2 mixture are shown in Fig. 4. Each experiment consisted of incrementally increasing the applied potential every hour and following the current as a function of time. The gaseous hydrogen product at the cathode was collected over a 10 min period; the volume of hydrogen gas recovered was equal within 5% to the integrated charge pumped across the membrane. The CO_2 concentration in the H_2 product was below our detection limit of 100 ppm. For applied voltages ≤0.2 V the current achieved steady state almost immediately and the MEA resistance ($R_{MEA} = V_{app}/I$) was constant. For applied voltages steps >0.24 V the current increased then decayed to steady state; the steady state R_{MEA} increased with increasing applied voltages. Increased MEA resistance with applied voltage was previously shown to result from water redistribution of water in the membrane due to electro-osmotic drag [40]. Steady state current achieves steady state after 1 h.

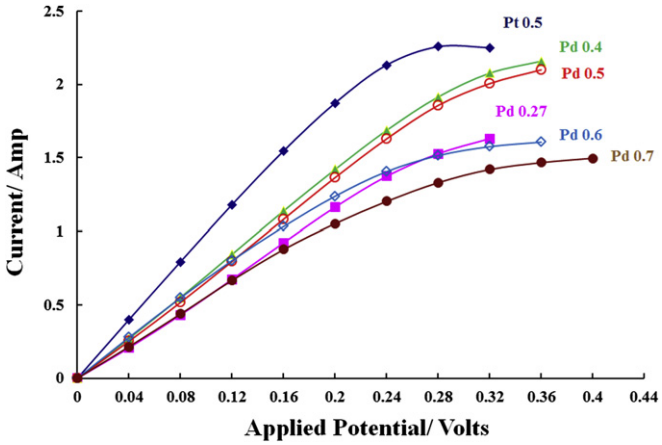

Fig. 2. Cyclic voltammograms after exposure of the working electrodes to CO_2/H_2 mixture of different C/H ratios at 0.2 V for 1 h. CV was performed on a 1.9 cm^2 active area MEA, in-situ. Scan rate 20 mV s^{-1} in the range of 0–1.2 V at 30 °C.

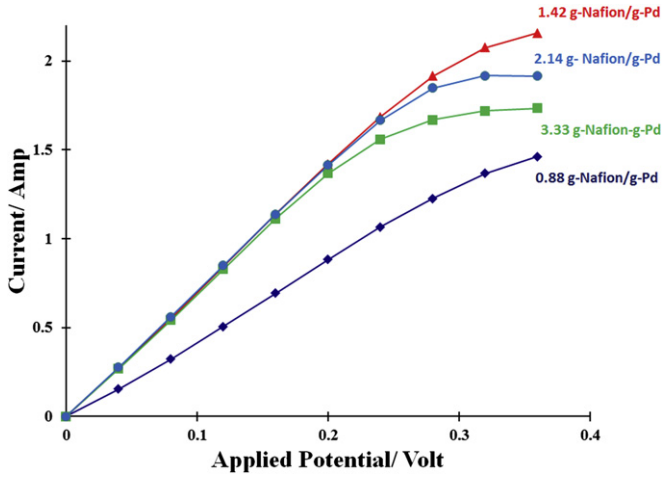

Fig. 3. Current as a function of applied potential for different Nafion loadings with a fixed Pd loading of 0.4 mg cm^{-2} and a carbon paper GDL.

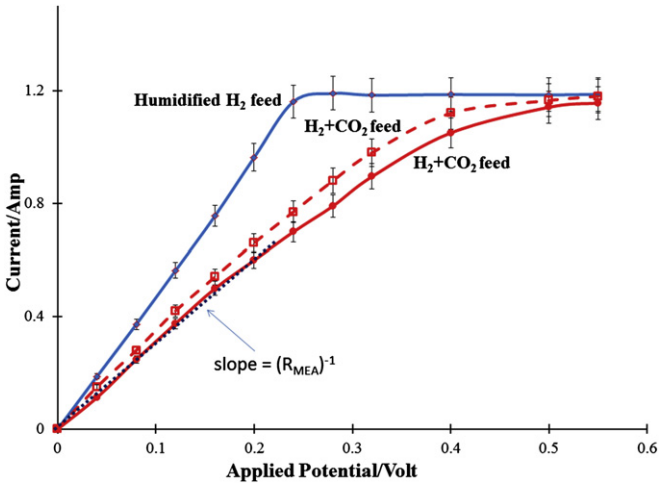

Fig. 5. Steady state current as function of applied potential, feed flow rate and feed composition for a Pd/C MEA. PEHP temperature = 50 °C. Solid blue line: 8.0 mL-H_2 min^{-1}, solid red line: 8.0 mL-H_2 min^{-1}/8.0 mL-CO_2 min^{-1}, dotted red line: 8.0 mL-H_2 min^{-1}/8.0 mL-N_2 min^{-1} (For interpretation of the references to color in this figure legend, the reader is referred to the web version of this article.).

Experiments were carried out with different anode feeds: (1) humidified H_2 feed; (2) humidified H_2 + N_2 feed; and (3) humidified H_2 + CO_2 feed. Steady state current and MEA resistance were measured as functions of applied potential and C/H and N/H ratios for Pt/C and Pd/C MEAs. Fig. 5 compares the steady state currents and R_{MEA} for $CO_2/H_2 = 1$ and $N_2/H_2 = 1$ mixtures as a function of applied potential for a Pd/C catalyst MEA. The current increased with applied voltage up to a maximum current; the maximum current is equal to the hydrogen feed rate to the anode, $I_{max} = (2Fq_{H_2})(60RT)^{-1}$. Current saturation is achieved at the lowest applied potential for pure H_2 feed. A larger applied potential is required to saturate the current when the H_2 is diluted with CO_2 or N_2. The voltage required for current saturation is greater when CO_2 is the diluent compared to N_2 as the diluent. The additional increase in potential caused by CO_2 is assumed to be due to CO_2 adsorption on the Pd [41].

At low potentials, the current is limited by the resistance to current flow across the membrane (ohmic limited current). Saturation current at high potentials corresponds to pumping all the hydrogen fed to the anode across to the cathode i.e. the saturation current is the stoichiometrically limited current. The effect of N_2 and CO_2 dilution on the current–voltage curves on Pt/C catalyst has been reported by other groups [12,14,30].

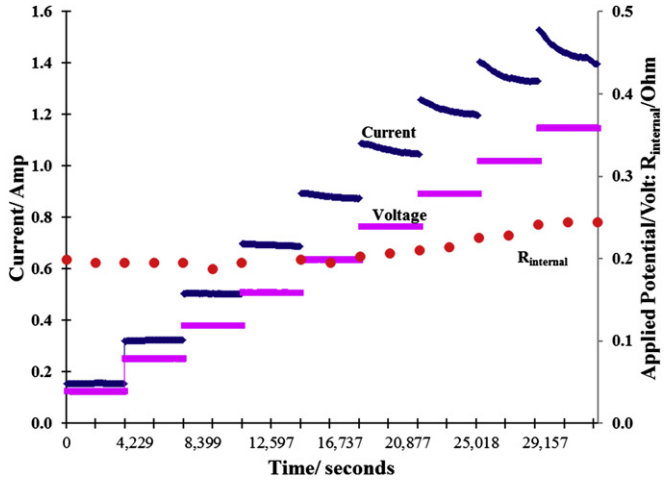

Fig. 4. Sample chronological data of the PEHP operation. The voltage was stepped every hour and the current was followed as a function of time. The membrane resistance was measured by current interrupt every 30 min (at the end of a cycle and half way through a cycle). The MEA had Pd/C catalysts at both the anode and cathode.

Table 3 provides a summary of the effective MEA resistances for Pd/C and Pt/C catalysts at an applied potential of 0.1 V measured as function of anode feed composition. Resistance was measured by current pulse relaxation and from the slope of the *IV* line. R_{MEA} determined from the *IV* slope is greater than R_{MEA} determined from current pulse relaxation. In addition, R_{MEA} from current pulse relaxation shows little change with anode composition whereas R_{MEA} increased by a factor of 2–3 as the hydrogen mole fraction at the anode decreased from 1 to 0.3.

The primary difference between Pd/C and Pt/C catalysts is that the effective MEA resistance is greater for the Pd/C catalyst. The effective resistance for the Pt/C MEA is ~0.1 Ω and the effective resistance of the Pd/C MEA is ~0.2 Ω. Both Pt/C and Pd/C MEAs show an increase in effective resistance with decreasing H_2 mole fraction of the anode feed. But the increase of the effective resistance is greater for Pd/C MEA. The saturation current is dependent only on the H_2 feed and is independent of the catalyst.

Abdulla et al. [12] presented a quantitative model that connected process parameters (flow rate, anode feed composition, temperature and applied potential) with hydrogen recovery and energy efficiency of the PEHP separation performed with a Pt/C catalyst. They showed that the hydrogen recovery and energy efficiency are given by equations (1) and (2), where the molar feed rate of hydrogen is given by $Q_H = (q_{feed}P)(60RT)^{-1}(1 + (C/H)_{feed})^{-1}$.

$$\text{Hydrogen Recovery} = \frac{I}{2FQ_{H_2}} \tag{1}$$

$$\text{Energy Efficiency} = \frac{\frac{I}{2F}\Delta H_{combustion} - IV_{app}}{Q_{H_2}\Delta H_{combustion}} \tag{2}$$

q_{feed} is the molar feed rate, F is Faraday's constant, I is the current, V_{app} is the applied potential and $\Delta H_{combustion}$ is the enthalpy of hydrogen combustion. Abdulla et al. showed that the maximum energy efficiency occurs at applied potentials at the transition between the ohmic current regime and the saturation current regime. Fig. 6 is a plot of the net energy efficiency for hydrogen

Table 3
Membrane electrode assembly resistances.

Catalyst C/H anode feed	MEA resistance current pulse (ohm)	MEA resistance *IV* slope (ohm)	Open circuit voltage (V)	$V = ((RT)/2F)\ln(x_H^{anode})/(x_H^{cathode})$
Pt/C C/H = 0	0.089	0.101	+ 0.0014	0
Pt/C C/H = 1/4	0.096	0.121	−0.0004	−0.0030
Pt/C C/H = 1/3	0.096	0.135	−0.0002	−0.0040
Pt/C C/H = 1/2	0.096	0.141	−0.0016	−0.0056
Pt/C C/H = 1/1	0.099	0.168	−0.0036	−0.0096
Pt/C C/H = 2/1	0.103	0.202	−0.0064	−0.0150
Pd/C C/H = 0	0.138	0.199	+ 0.0009	0
Pd/C C/H = 1/4	0.138	0.221	+ 0.0025	−0.0030
Pd/C C/H = 1/3	0.143	0.267	+0.0021	−0.0040
Pd/C C/H = 1/2	0.141	0.317	+0.0026	−0.0056
Pd/C C/H = 1/1	0.145	0.333	−0.0025	−0.0096
Pd/C C/H = 2/1	0.145	0.409	−0.0058	−0.0150
Pt/C N/H = 0	0.089	0.101		
Pt/C N/H = 1/4	0.094	0.114		
Pt/C N/H = 1/3	0.096	0.127		
Pt/C N/H = 1/2	0.098	0.135		
Pt/C N/H = 1/1	0.099	0.148		
Pt/C N/H = 2/1	0.105	0.180		
Pd/C N/H = 0	0.138	0.199		
Pd/C N/H = 1/4	0.140	0.215		
Pd/C N/H = 1/3	0.140	0.250		
Pd/C N/H = 1/2	0.140	0.280		
Pd/C N/H = 1/1	0.141	0.295		
Pd/C N/H = 2/1	0.143	0.360		

recovery with Pt/C and Pd/C MEAs at two different C/H ratios. The larger effective resistance of the Pd/C MEA results in lower net energy efficiency and larger applied voltages are required to achieve the same hydrogen recovery.

3.3. Effect of CO_2 on the active electrocatalyst surface area

The results summarized in Table 3 showed that the effective MEA resistance increased more as H_2 was diluted with CO_2 than with N_2, suggesting CO_2 adsorption reduced the electrochemical active surface area (ESA) increasing the effective MEA resistance. ESA for the MEA anode was determined by cyclic voltammetry (CV). The cathode was a Pt/C catalyst exposed to humidified hydrogen serving as a standard hydrogen reference electrode (SHE). The anode was exposed to humidified H_2/CO_2 at open circuit and then flushed with humidified N_2. The voltage was then ramped from 0 to 1.2 V vs. SHE and then ramped down to 0 V. The CVs for the Pt/C and Pd/C MEAs are shown in Figs. 7 and 8. The potentiodynamic curves for Pt/C and Pd/C electrodes have the typical forms for these metals [42]. The peaks at low-potential (below 0.4 V) are associated with oxidation and reduction of hydrogen. Hydrogen is adsorbed on Pt, but hydrogen is both adsorbed and absorbed with Pd. The different peaks observed in this region have been shown to result from different crystal orientations of the polycrystalline catalyst present on the electrode. Between 0.45 and 0.65 V, there is a small constant current from double-layer charging; no significant electrochemical reactions occur at these potentials. The region at potential higher than 0.7 V represented the oxygen evolution reaction. As the potential was then swept backward to zero, oxygen and Pt–O or Pd–O reduction reactions occurred, followed by hydrogen adsorption reactions.

The CV curves for Pt/C catalysts show very little difference as the concentration of CO_2 at the anode is increased. In contrast, hydrogen oxidation and Pd–O reduction peaks are both reduced in the presence of CO_2 with Pd/C anode catalyst, suggesting that CO_2 adsorbs more strongly to Pd than Pt inhibiting adsorption of both hydrogen and water. CO_2 reduction was not detected in the potential range of 0.7–0.9 V. Previous studies have reported CO_2 reduction [43]. We suggest that CO_2 was probably too small to distinguish from water oxidation/reduction.

Hydrogen desorption is frequently used to estimate the electrochemical active surface area (ESA) of Pt [44]. Because it was not possible to unambiguously distinguish between adsorbed and absorbed hydrogen on Pd. The ESAs of Pd and Pt were estimated from the Pt–O and Pd–O reduction peaks [45]. The baselines for oxidation and reduction peaks were interpolated from the double layer charging region and the integrated charge under the metal oxide reduction peaks was calculated; the ESAs are summarized in Table 4. The charges from the CV measurements were converted into surface areas by assuming each Pt or Pd surface atom adsorbed one oxygen atom. ESA decreased with the increasing C/H ratio for both Pt/C and Pd/C catalysts, but the effect was much greater for Pd catalysts.

The calculated electroactive surface areas show some discrepancy with the metal surface areas provided by the vendor. ESAs for Pt/C and Pd/C catalysts were both larger than the surface areas

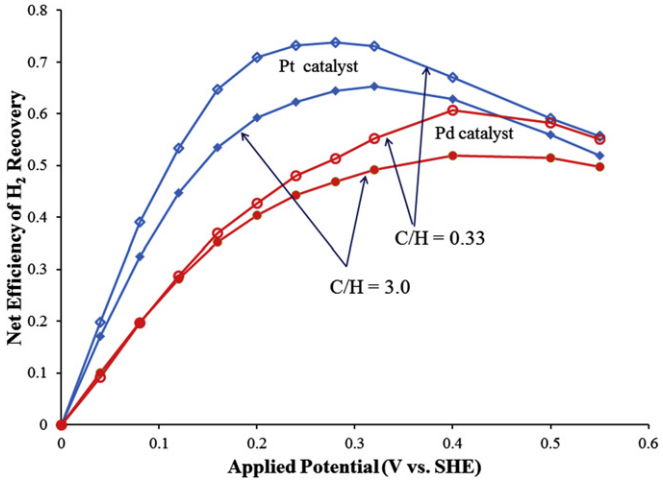

Fig. 6. Net energy efficiency for hydrogen purification with a PEHP as functions of applied potential and C/H ratio of the anode feed.

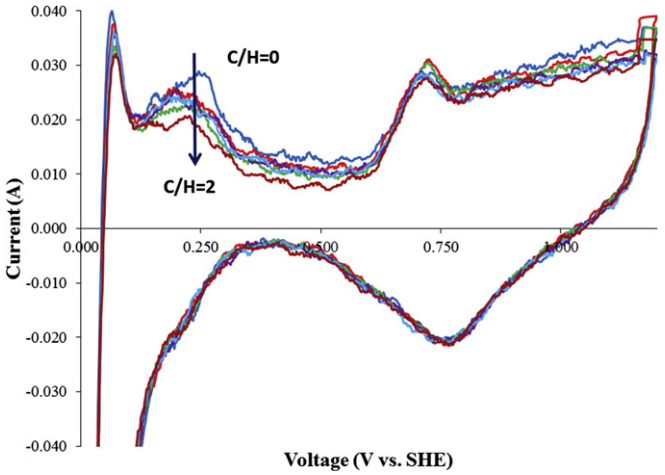

Fig. 7. Cyclic voltammograms for Pt/C anode MEA at 30 °C, with different C/H compositions.

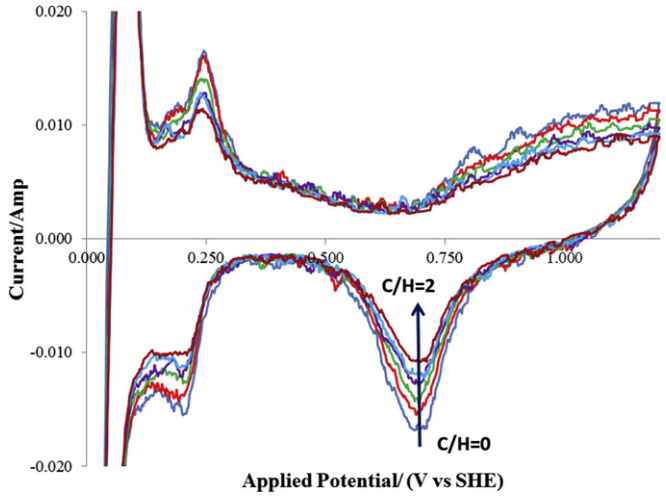

Fig. 8. Cyclic voltammograms for Pd/C anode MEA at 30 °C, with different C/H compositions.

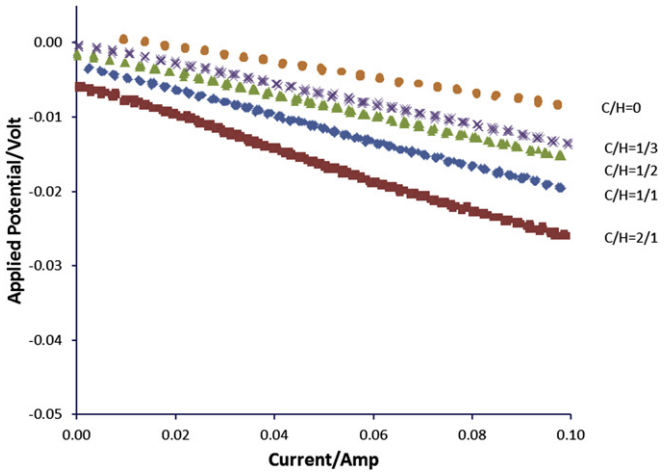

Fig. 9. Polarization curves (*IV*) for Pt/C MEAs. $T = 50$ °C, anode feed 16 mL min^{-1} total flow, with CO_2/H_2 ratio as specified.

suggested by Premetek. ESA for Pt/C was larger than for Pd/C which is opposite that suggested by the vendor. There is no obvious explanation for these differences.

Metal particle sizes were estimated from the ESA: $d_{particle} = (6M_{catalyst}/\rho_{Metal}A)$, where $M_{catalyst}$ is the mass of metal catalyst and A is the ESA of the metal. The Pt particle size is estimated to be 3.2 nm (compared to 2.5 ± 0.3 nm reported by the vendor), and the Pd particle size is 5.3 nm (compared to 3.5 ± 0.5 nm) reported by the vendor.

3.4. Effect of CO_2 on electrode polarization

Figs. 9 and 10 show polarization curves obtained for (Pd/C)/Nafion/(Pt/C) and (Pt/C)/Nafion/(Pt/C) MEAs as functions of the C/H ratio of the anode feed with a fixed total flow rate at the anode of 16 cm^3 min^{-1}. The cathode was humidified hydrogen in all cases; the Pt/C cathode served as a hydrogen reference electrode. The current was measured during potentiometric sweeping from 0 to 0.04 V. The MEA resistance was measured by pulsed current relaxation before and after each voltage sweep. The anode composition was assumed to be equal to the feed composition; the maximum current was 0.1 A, corresponding to <4% consumption of the H_2 feed to the PEHP.

For $I > 0$ the polarization curves were nearly straight lines. The slope of the *IV* line is the effective MEA resistance for the protonic current. The intercept is the sum of the activation potentials for H_2 oxidation at the anode and H^+ reduction at the cathode and the potential difference of hydrogen at the anode and cathode. Table 3 summarizes the MEA resistance from the pulsed current relaxation, the effective MEA resistance from the polarization curve, and the potential at zero current for the Pt/C and Pd/C MEAs at different C/H ratios.

The MEA resistances evaluated from the pulsed current relaxation were nearly constant with C/H ratio for both Pt/C and Pd/C MEAs, but the Pd/C MEA resistance was 40% larger than the Pt/C MEA resistance. The effective MEA resistances determined from the slopes of the *IV* curves were larger than the pulsed current relaxation. In addition, the effective MEA resistances determined from the polarization curves increased with increasing C/H ratio. The increased resistance was larger for the Pd/C MEA than for the Pt/C MEA.

The open circuit voltages decreased from 1 mV to −6 mV with increasing C/H ratio. The open circuit voltages were expected to decrease with composition; the open circuit Nernst potentials were calculated and listed in Table 3.

The open circuit voltages were greater than the predicted Nernst potentials. We suggest that this is the result of molecular hydrogen crossover from the cathode to the anode reducing the hydrogen activity difference between the anode and cathode. The decrease in

Table 4
Electroactive surface area of Pt/C and Pd/C electrodes.

Catalyst	CO_2/H_2	ESA (m^2 g-catalyst)
Pt/C	0	56
Pt/C	1/4	53
Pt/C	1/3	53
Pt/C	1/2	52
Pt/C	1/1	49
Pt/C	1/2	48
Pd/C	0	40
Pd/C	1/4	35
Pd/C	1/3	31
Pd/C	1/2	28
Pd/C	1/1	26
Pd/C	1/2	24

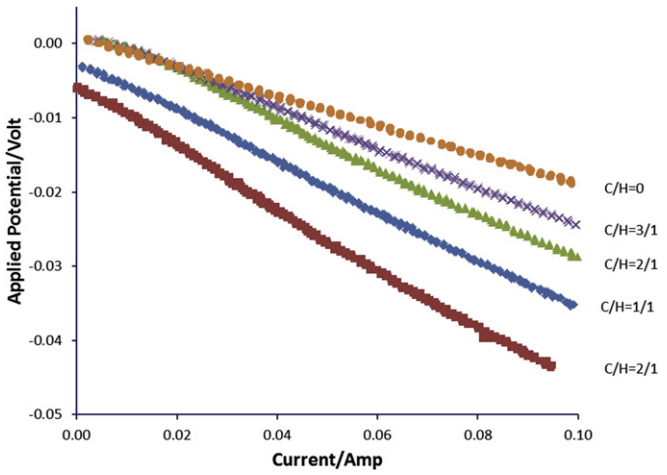

Fig. 10. Polarization curves (*IV*) for Pd/C MEAs. $T = 50$ °C, anode feed 16 mL min^{-1} total flow, with CO_2/H_2 ratio as specified.

the open circuit potential with increasing C/H ratio was less than that predicted by the Nernst potential, which is also consistent with greater H_2 crossover at larger activity difference.

Activation potentials for the hydrogen oxidation reaction (HOR) are <10 mV. Other researchers have also reported activation potentials for Pt/C electrodes of 5–10 mV [15,22,30]. Surprisingly, dilution of H_2 by CO_2 had a negligible effect on the activation potential but caused the ohmic potential to increase. Other researchers have also reported larger potential ohmic potential losses resulting from dilution of the H_2 with an inert gas [39,43]. Those ohmic potential losses due to CO_2 appear to be much greater than any activation potential losses for hydrogen oxidation and reduction.

4. Discussion

The results showed that a polymer electrolyte hydrogen pump can effectively recover hydrogen from CO_2/H_2 mixtures with a Pd/C catalyst. Fig. 7 shows that for equal mass loading a Pd/C catalyst MEA had ~80% the energy efficiency of a Pt/C MEA. If the only potential drop in the PEHP was the ohmic potential drop then the efficiency of the Pd/C PEHP could be increased to match the Pt/C PEHP by increasing the MEA area by 20%. Pd is approximately 1/3 the cost of Pt so even with the 20% increase in MEA area a Pd/C catalyst would substantially reduce the cost of the PEHP.

If the Pd/C catalyst had larger activation potential than Pt/C for hydrogen oxidation and reduction then increasing the MEA area would not improve the energy efficiency for hydrogen separation. Polarization data indicated that the HOR activation potentials for Pd/C and Pt/C catalysts were negligibly small which is promising for the Pd/C catalysts. But the ohmic potentials were greater for Pd/C MEAs than for Pt/C MEAs, which could pose a problem. If we seek to replace Pt/C catalysts with Pd/C catalysts we need to identify the source of the potential drop across the MEA to see if it can be overcome. Three key experimental results must be accounted for:

1. The MEAs all used the same thickness Nafion membrane which should have the same ohmic resistance. *Why were the ohmic resistances dependent on the catalyst?*
2. Polarization data showed that the dilution of H_2 at the anode with CO_2 or N_2 caused the effective resistance of the MEA to increase. *Why should the gas phase composition change in the membrane resistance?*
3. The effective MEA resistance determined from polarization measurements increased by 200% due to hydrogen dilution at the anode, but the MEA resistance determined by pulsed current relaxation only changed by 10%. *Why should the apparent membrane resistance depend on measurement technique?*

Changes of MEA resistance due to changes in gas composition must be associated coupling of H_2 and proton transport in the catalyst layer. Hydrogen transport through the gas phase in the pores of the catalyst layer is balanced by proton transport through the Nafion layer covering the catalyst.

A simplified pore model for the anode catalyst layer in the hydrogen pump is illustrated in Fig. 11. The catalyst layer consists of carbon particles, typically ~30 nm in diameter with 2–4 nm Pt or Pd particles supported on the carbon particles. Nafion is mixed with the catalyst particles; the Nafion forms a film over the surface of the carbon particles. H_2 diffuses through the pores of the catalyst layer, and then across the thin Nafion film to the metal catalyst. H_2 is oxidized on the surface of the metal catalyst and the protons formed are transported through the Nafion film. To model the catalyst layer we assume the catalyst layer consists of an electrically conducting carbon matrix of thickness L with cylindrical pores with radius r_{pore} that extend between the anode gas diffusion layer and the membrane. The pore surfaces are decorated with Pt or Pd particles. The metal particles and the carbon pore surface are coated with a thin film of Nafion. The physical parameters that describe the catalyst layer are listed in the Nomenclature table.

4.1. Coupling of diffusion and proton transport in the catalyst layer

Gas phase hydrogen diffuses from the anode gas flow channel and the gas diffusion layer (GDL) to the catalyst layer (CL) in the z-direction. The H_2 flux through the gas diffusion layer is constant. Protons are generated on the surfaces of the Pt particles throughout the catalyst layer. The H_2 flux decreases between the GDL/CL interface and the CL/membrane interface while the proton flux (current) increases. At steady state the decrease in the H_2 molar flux in the z-direction is equal to increase in proton flux divided by $2F$. At any z-plane the increase in proton current in the z-direction is equal to the hydrogen across the Nafion film in the x-direction. The local hydrogen concentrations in the gas phase, P_H and in the membrane, c_H are connected by phase equilibrium by a Henry's law constant ($c_H = K_H P_H$). Equation (4) shows the mass balances for a single pore; these mass balances are generalized to the catalyst layer in equation (5). Ordinary differentials have been employed in equations (4) and (5). It is assumed that there are no radial variations in H_2 pressure or current density. Only the H_2 concentration in the thin Nafion film is assumed to vary in both x and z directions.

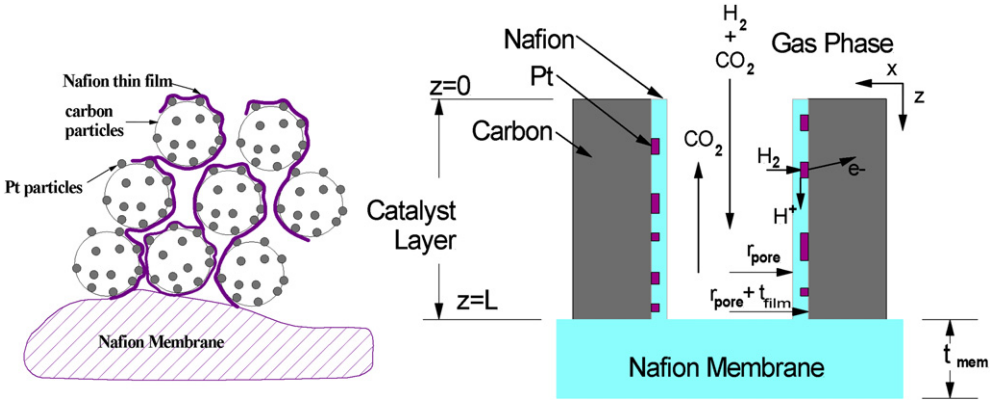

Fig. 11. Schematic model of catalyst layer for PEHP. The drawing at the left shows the carbon particles supporting Pt or Pd nanoparticles with a thin film of Nafion coating the particles. At the right is a pore model showing dimensions for the pores, and Nafion film.

$$\{\text{change in flux in pore}\} = \{\text{flux across Nafion film}\} = \{\text{change in current density in Nafion film}\} \quad (3)$$

$$-\frac{\pi r_{\text{pore}}^2 D_g}{RT}\frac{d^2 P_H(z)}{dz^2} = -2\pi r_{\text{pore}} D_f \frac{\partial c_H(z)}{\partial x} = \frac{2\pi r_{\text{pore}} r_{\text{film}}}{2F}\frac{dj}{dz} \quad (4)$$

$$-\frac{\varepsilon D_g}{RT}\frac{d^2 P_H}{dz^2} = -\frac{\phi A_{\text{cat}} M_{\text{cat}}}{w_M} D_f \frac{dc_H}{dx} = \frac{\phi A_{Nx}}{2F}\frac{dj}{dz} \quad (5)$$

The boundary conditions are,

$$\begin{aligned} &P_H = P_H^0 \quad \text{at} \quad z = 0 \\ &\frac{dP_H}{dz} = 0 \quad \text{at} \quad z = L \\ &j = 0 \quad \text{at} \quad z = 0 \\ &\frac{\partial c_H}{\partial x} = \text{rate}(P_H, dV/dz) \quad \text{at} \quad x = t_{\text{film}} \end{aligned} \quad (6)$$

An additional mass balance constraint is that the current in the z-direction at the membrane/catalyst layer interface ($z = L$) is equal to the total current through the membrane and the external load. The coupled differential equations can be solved numerically once an appropriate rate expression is defined at the Nafion film–electrode surface; this rate is a function of the unknown local concentration of H_2 and local electrode potential. Simple analytic expressions for the concentrations and fluxes can be obtained if we assume the H_2 transport rate across the Nafion film in the x-direction is constant. As specified by equation (7) the H_2 flux in the x-direction at position z is constant if there is a non-zero hydrogen concentration in the gas phase, and zero if the gas phase H_2 concentration is zero.

$$\{H_2 \text{ flux in x-direction @ z}\} = \frac{\phi A_{\text{cat}} M_{\text{cat}}}{w_M} D_f \frac{dc_H}{dx} = \begin{cases} f_H V_{\text{app}} & \text{at } P_H(z) > 0 \\ 0 & \text{at } P_H(z) = 0 \end{cases} \quad (7)$$

Equation (7) approximates the flux when hydrogen oxidation kinetics are fast and diffusional transport across the Nafion thin film is the limiting rate process. The activation potential at the anode was shown to be <10 mV, so equation (7) should be a reasonable approximation for applied potentials >100 mV.

The catalyst layer is assumed to consist of uniform parallel pores. A fraction ϕ of the pores surface is covered with Pd or Pt and is electrochemically active. We assume that only surfaces coated with active catalyst carry the proton current; pores without active catalyst carry no proton current. The constant hydrogen flux across the Nafion film in the x-direction implies that the current density increases linearly from 0 at the GDL/CL interface to the J_0 at the CL/membrane interface, and remains constant as J_0 across the membrane. In thick catalyst layers the current density increases linearly from the GDL/CL interface to a location partway through the catalyst layer at which all the H_2 has been reacted. We will only consider the thin catalyst layer approximation here.

We seek to find the relationship between the current and applied potential. The current at position z between the GDL/CL interface ($z = 0$) and the CL/membrane interface ($z = L$) is found by integrating equation (5).

$$j_{\text{cat}}(z) = 2F f_H V_{\text{app}} \phi A_a \frac{z}{L} \quad (8)$$

The total current must be continuous at the CL/membrane interface so $J_0 = 2F f_H V_{\text{app}} \phi A_a$.

The potential difference across the membrane is $\Delta V_{\text{mem}} = J_0 R_{\text{mem}}$, where $R_{\text{mem}} = \rho_H t_{\text{mem}}$ is the areal membrane resistance and ρ_H is the resistivity of Nafion.

The resistance for proton transport in the catalyst layer is equal to Nafion's resistivity multiplied by the catalyst layer thickness divided by the fractional area of the Nafion in a z-plane, A_{Nx}, as given by equation (9).

$$R_{CL} = \frac{\rho_H L}{\phi A_{Nx}} = \frac{\rho_H}{\phi}\frac{\left(\frac{M_{\text{cat}}}{(1-\varepsilon) w_M \rho_c}\right)}{\left((1-\varepsilon) w_M w_N \frac{\rho_c}{\rho_N}\right)} = \frac{\rho_H}{\phi}\frac{2\times 10^{-3}\text{cm}}{0.17\text{cm}^2 - \text{Nafion.cm}^{-2}} \quad (9)$$

There are two contributions to the ohmic potential difference for proton transport across the MEA: (1) the potential difference across the catalyst layer due to average proton current through the thin Nafion film covering the catalyst particles; and (2) the potential difference for current flow across the membrane. The average current is $J_0/2$ in the catalyst layer.

$$V_{\text{ohmic}} = \frac{J_0}{2} R_{CL} + J_0 R_{\text{mem}} = J_0 \rho_H \left[\frac{L}{2}\frac{1}{\phi A_{Nx}} + t_{\text{mem}}\right] \quad (10)$$

In addition to the ohmic potential loss across the catalyst layer there is a Nernst potential difference across the catalyst layer resulting from the difference in hydrogen activity. The Nernst potential is given by equation (11) where the x refers to hydrogen mole fractions.

$$V_{\text{Nernst}} = \frac{RT}{2F}\ln\left[\frac{a_H^{\text{GDL/CL}}}{a_H^{\text{CL/mem}}}\right] = \frac{RT}{2F}\ln\left[\frac{x_{H_2}^{\text{GDL/CL}}}{x_{H_2}^{\text{CL/mem}}}\right] \quad (11)$$

The composition across the catalyst layer is found by solving the coupled diffusion for H_2 transport in the gas pores and proton transport in equation (Eq. (12)) with the boundary conditions given in equation (6). The H_2 flux across the Nafion film in the x-direction is equal to the current density gradient in the z-direction, $(dj/dz) = 2F f_H$.

$$\begin{aligned} &\frac{\varepsilon D_g P}{RT}\frac{d^2 x_{H_2}}{dz^2} = \frac{A_{Nx}}{2F}\frac{dj}{dz} \\ &\frac{d^2 x_H}{d\zeta^2} = \alpha J_0 \end{aligned} \quad (12)$$

where

$\zeta = (z/L)$

$\alpha = (LRTA_{Nx})/(2F\varepsilon D_g P A_a)$.

The hydrogen mole fraction is given by equation (13), which is substituted into equation (11) to obtain the Nernst potential difference.

$$x = x_0 - \alpha J_0\left(\zeta - \frac{\zeta^2}{2}\right) \quad (13)$$

$$V_{\text{Nernst}} = \frac{RT}{2F}\ln\left[\frac{x_H(\zeta = 1)}{x_H(\zeta = 0)}\right] = \frac{RT}{2F}\ln\left[\frac{x_0 - \alpha J_0}{x_0}\right] \approx \frac{RT}{2F}\frac{\alpha J_0}{x_0} \quad (14)$$

The applied potential to the hydrogen pump is equal to the sum of the ohmic potentials and the Nernst potential.

$$V_{\text{app}} = V_{\text{ohmic}} + V_{\text{Nernst}} = J_0 \rho_H \left[\frac{L}{2}\frac{1}{\phi A_{Nx}} + t_{\text{mem}}\right] + \frac{RT}{2F}\frac{\alpha J_0}{x_0} \quad (15)$$

The effective MEA resistance for the hydrogen pump is the ratio of the applied voltage to the current as shown in equation (16).

$$\begin{aligned} R_{\mathrm{MEA}} &= \left[\frac{L}{2}\frac{1}{\phi A_{\mathrm{Nx}}} + t_{\mathrm{mem}}\right]\rho_{\mathrm{H}} + \frac{RT}{2F}\frac{\alpha}{x_0} \\ &= t_{\mathrm{mem}}\rho_{\mathrm{H}} + \left\{\frac{\rho_{\mathrm{N}}}{2(1-\varepsilon)^2 w_{\mathrm{M}}^2 \rho_{\mathrm{c}}}\right\}\rho_{\mathrm{H}}\left[\frac{M_{\mathrm{cat}}}{w_{\mathrm{N}}}\right] \\ &+ \left\{\left(\frac{RT}{2F}\right)^2 \frac{w_{\mathrm{M}}}{A_{\mathrm{cat}}\rho_{\mathrm{N}}\varepsilon D_{\mathrm{g}}\phi}\right\}\left[\frac{w_{\mathrm{N}}}{x_{\mathrm{H_2}}P}\right] \\ &= \{\text{membrane resistance}\} \\ &+ \{\text{proton resistance in catalyst layer}\} \\ &+ \{\mathrm{H_2}\text{ diffusion in catalyst layer}\} \end{aligned} \tag{16}$$

The terms in equation (16) are the resistances associated with (1) proton transport in the membrane, (2) proton transport in the catalyst layer, and (3) hydrogen transport in the pores of the catalyst layer. Based on the catalyst layer parameters listed in Nomenclature section all three contributions are comparable in value: (1) membrane resistance = 0.10 Ω cm^{-2}; (2) catalyst layer resistance = 0.09 Ω cm^{-2}; (3) diffusional resistance = 0.02 Ω cm^{-2}@x_{H2} = 0.5 and 0.15 Ω cm^{-2}@x_{H2} = 0.12.

The concentration and flux profiles across the catalyst layer are displayed graphically in Fig. 12. These profiles were based on the thin catalyst layer approximation and the assumption of a constant H_2 flux across the Nafion film in the catalyst layer. The proton current increases linearly across the catalyst layer, and then is constant in the membrane. The linear increase in the proton current produces a quadratic increase of the ohmic potential from the gas/catalyst layer interface to the catalyst layer/membrane interface. The ohmic potential then increases linearly across the membrane. The H_2 flux decreases across the catalyst layer which results in a compositional potential increase.

4.2. Effect of catalyst loading and hydrogen concentration on MEA resistance

The model predicts that the effective MEA resistance increases with increased catalyst loading, increases with decreasing hydrogen mole fraction, decreases with increased electrochemically active catalyst and can either increase or decrease with Nafion loading.

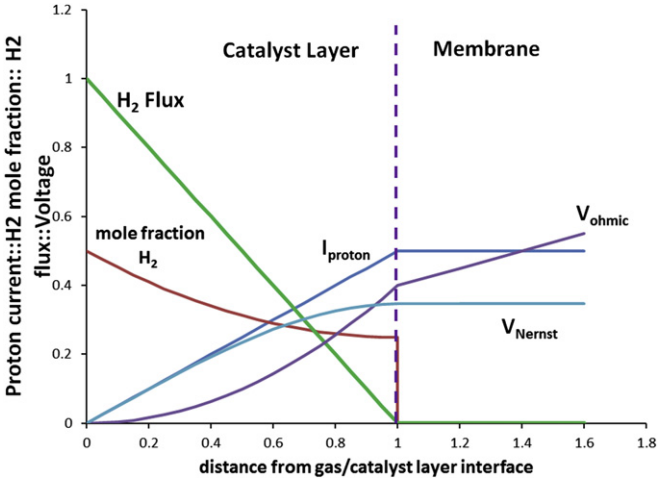

Fig. 12. Concentration, flux and potential profiles in the cathode catalyst layer.

1. The resistance increases with catalyst loading because the distance for proton transport across the catalyst layer increases. The increased MEA resistance is evident in Fig. 2. The slope of the *IV* curve, which is equal to $1/R_{\mathrm{MEA}}$, decreases with increased catalyst loading.
2. R_{MEA} decreases with Nafion loading. The thin Nafion film in the pores gets thicker so it presents less resistance to proton transport. At higher Nafion loadings the decreased resistance to proton transport in the *z*-direction is offset by increased resistance to H_2 diffusion in the *x*-direction.
3. The effective MEA resistance increases with decreasing H_2 mole fraction. The diffusional resistance increases inversely with hydrogen mole fraction.
4. The effective MEA resistance increases due to a reduction of electroactive surface area resulting from CO_2 adsorption. Fig. 13 shows the effective MEA resistances determined from the polarization data as functions of the reciprocal of ESA determined from CV for both the Pt/C and Pd/C MEAs. Both sets of data fall on the same line as predicted by equation (16). Fig. 14 shows the MEA resistances as functions of the reciprocal of the hydrogen mole fraction. The data for both Pt and Pd show the resistance increases with decreasing hydrogen mole fraction. The two sets of data fall on different lines because the two catalysts have different intrinsic ESAs.

4.3. Electrical resistance and gas phase diffusion

The effective MEA resistances determined from the polarization curves were larger than those determined by pulsed current relaxation measurements. Current interrupt measures the "instantaneous" voltage response to an applied current pulse at short times when no redistribution of species can occur by diffusion. Current interrupt measurements respond to frozen concentration gradients of H_2 in the pores and H^+ in the Nafion in both the catalyst layer and the membrane. The effective MEA resistances obtained from the polarization curves are obtained over periods of 10–1000 s such that H_2 in the catalyst layer pores and H^+ in the catalyst layer Nafion have time to redistribute by diffusion. Hence the effective MEA resistance from polarization measurements includes the resistance from the proton transport in the membrane, gas transport in the catalyst layer and proton transport in the catalyst layer.

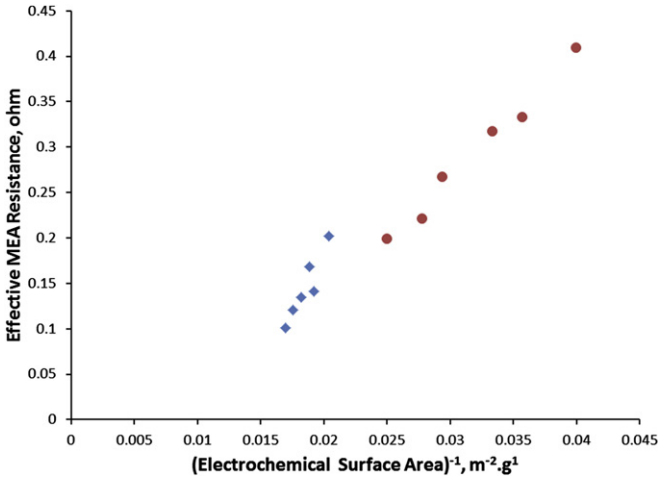

Fig. 13. Effective MEA resistances as functions of 1/(electrochemical active surface area). The blue diamonds are the data from Pt/C catalysts and the red circles are for Pd/C catalysts (For interpretation of the references to color in this figure legend, the reader is referred to the web version of this article.).

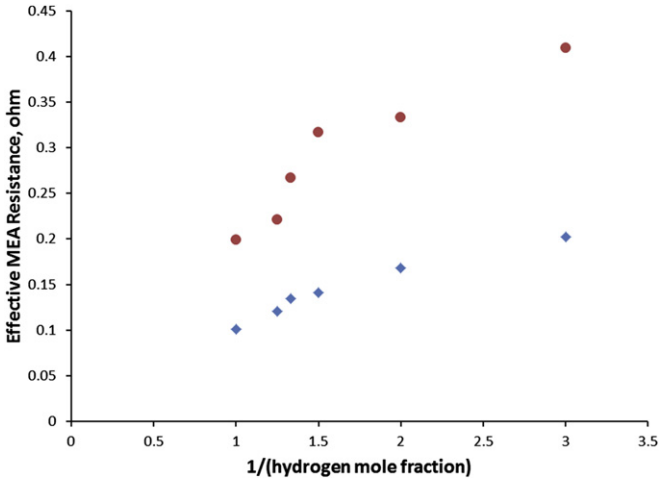

Fig. 14. Effective MEA resistances as functions of 1/(hydrogen mole fraction in anode gas phase). The blue diamonds are the data from Pt/C catalysts and the red circles are for Pd/C catalysts (For interpretation of the references to color in this figure legend, the reader is referred to the web version of this article.).

4.4. Consequences for catalyst layer improvement

The original goal of our experiments was to see if Pd would be a suitable replacement for Pt in a polymer electrolyte hydrogen pump for separating H_2/CO_2 mixtures. The results from this study initially suggested that Pd/C catalysts would result in lower energy efficiency than Pt/C catalysts. Upon closer examination it was discovered that the lower efficiency was not a result of the intrinsic catalytic activity of Pd vs. Pt, but rather the result of differences in CO_2 sorption by Pd and Pt and differences in the metal dispersion on the carbon support. Modification of the catalyst preparation to improve Pd dispersion could improve the performance of Pd/C catalysts in a PEHP. The commercial 20 wt% Pd/C catalysts had reduced electroactive catalyst area compared to the 20 wt% Pt/C catalyst we employed. If the dispersion of the Pd was improved to be the same as Pt the two catalysts would be closer in performance.

The Pd catalysts will always suffer more than Pt catalysts from poisoning by CO_2 adsorption. That penalty from CO_2 adsorption on Pd is small at small CO_2/H_2 ratios and becomes more significant at larger CO_2/H_2 ratios. Improved efficiency at reduced cost could be achieved with a multistage separation unit as described by Abdullah et al. [12] employing Pd catalyst in the early stages where the CO_2/H_2 ratio is small and only using Pt in the later stages where the CO_2/H_2 ratio is large.

5. Conclusions

Electrochemical properties and hydrogen pump performances were investigated for Pt/C and Pd/C catalysts for hydrogen separation from CO_2/H_2 mixture. The electrochemical active surface area was smaller on Pd/C catalyst than on Pt/C catalyst, which resulted in a larger effective MEA resistance with the Pd/C catalyst MEA. There was greater CO_2 sorption on Pd than Pt, further reducing the electroactive catalyst surface area at high CO_2/H_2 ratios which caused greater reduction of the separation efficiency. It would be possible to replace Pt by Pd in hydrogen pump separations for the purpose of lowering cost but this would be accompanied by reduced energy efficiency. Energy efficiency could be improved by staged operations using Pd in the early stages at low CO_2/H_2 ratios and using Pt in the final stages where the CO_2/H_2 ratio is large.

CO_2 affected both Pt/C and Pd/C catalysts not only by poisoning active catalyst sites but also by reducing the mass transport of hydrogen through the pores of the catalyst layer. An anode transport model that included the coupling of proton transport through the catalyst layer, proton transport through the membrane and hydrogen transport through the catalyst layer showed that hydrogen depletion in gas mixtures creates a potential resistance across the catalyst layer that shows up as an effective resistance. The transport model shows that the effective MEA resistance increases with increased catalyst loading, decreases with increased Nafion loading, and decreases with increased electrochemical active surface area. Compared with Pt/C, Pd/C catalyst exhibited lower resistance to CO_2 poisoning, higher effective ohmic resistance and lower mass transport coefficient of hydrogen, which can be related to the different intrinsic properties of the catalytic metal and the different micro-structures of the catalyst layer. Improved preparation of the supported metal catalysts should be investigated further to achieve optimal PEHP performance for practical applications.

Acknowledgments

The authors thank the NSF (CBET 0754715) for support of this work. Dr. Wu thanks the NSFC (21176044) and the Chinese Scholarship Council for support to work at Princeton University. The authors thank May Jean Cheah for her assistance in preparing membrane electrodes and building up the experimental setup in this work.

Nomenclature

A_a	surface area of pores per geometric surface area ($0.625\ m^2\ cm^{-2}$)
A_{cat}	surface area of catalyst ($\sim 250\ m^2\ g\text{-}cat^{-1}$)
A_E	electroactive surface area ($\sim 50\ m^2\ g\text{-}cat^{-1}$)
a_H	activity of gaseous hydrogen
A_{Nx}	fractional cross-sectional area of Nafion in catalyst layer ($0.17\ cm^2\text{-Nafion}\ cm^{-2}$)
c_{H2}	concentration of H_2 in the Nafion film in the catalyst layer ($mol\ cm^{-3}$)
D_f	hydrogen diffusivity in Nafion thin film ($\sim 10^{-7}\ cm^2\ s^{-1}$)
D_g	gas phase diffusivity of hydrogen in pores ($\sim 10^{-2}\ cm^2\ s^{-1}$)
F	Faraday's constant 96,478 C mol^{-1}
$\Delta H_{combustion}$	hydrogen combustion enthalpy ($-286\ kJ\ mol^{-1}$)
I	current (A)
I_{max}	saturation current (A)
$j(z)$	local current density in the catalyst layer ($A\ cm^{-2}$)
J_0	proton current density through membrane ($A\ cm^{-2}$)
K_H	Henry's law constant for H_2 solubility in Nafion membrane
L	thickness of the catalyst layer ($\sim 20 \times 10^{-4}$ cm)
M_{cat}	weight loading of metal catalyst per geometric area ($\sim 5 \times 10^{-4}\ g\text{-Pt}\ cm^{-2}$)
P	gas phase pressure
P_H	hydrogen partial pressure
q_{feed}	anode feed rate ($cm^3\ min^{-1}$)
Q_{H_2}	molar hydrogen feed rate ($mol\ s^{-1}$)
R	gas constant ($8.314\ J\ mol^{-1}\ K^{-1}$, $82.05\ cm^3\ bar\ mol^{-1}\ K^{-1}$)
R_{CL}	catalyst layer resistance (Ω)
R_{mem}	membrane resistance (Ω)
R_{MEA}	membrane electrode assembly resistance (Ω)
r_{Metal}	supported metal particle size ($\sim$2.5–3.5 nm)
$r_{particle}$	carbon catalyst support particle size ($\sim$30 nm)
r_{pore}	pore diameter in catalyst layer ($\sim$10 nm)

t_{film}	thickness of Nafion film on the catalyst particles $t_{film} = (w_N w_M)/(\rho_N A) \approx 1–2$ nm
t_{mem}	thickness of Nafion membrane (125 μm)
V_{app}	applied potential (V)
V_{Nernst}	Nerst potential difference
V_{ohmic}	ohmic potential difference
w_M	weight fraction of metal (0.2 g-Pt or Pd/g-catalyst)
w_N	weight fraction of Nafion (g-Nafion/g-(Pd or Pt))
x_{H_2}	hydrogen mole fraction in gas
α	1/characteristic current density at catalyst layer/membrane interface
ε	void fraction of catalyst layer ($\sim$0.4)
ρ_c	density of catalyst particles ($\sim$2 g cm^{-3})
ρ_N	density of Nafion (2 g cm^{-3})
ϕ	fraction of surface area that is electrochemically active
ζ	dimensionless distance in catalyst layer

References

[1] W.F. Baade, U.N. Parekh, V.S. Raman, Hydrogen, in: Kirk–Othmer Encyclopedia of Chemical Technology, vol. 13, Wiley, New York, 2004, pp. 759–808.
[2] J.D. Holladay, J. Hu, D.L. King, Y. Wang, Catalysis Today 139 (4) (2009) 244–260.
[3] T. Riis, E.F. Hagen, P.J.S. Vie, Ø Ulleberg, Hydrogen Production and Storage – R&D Priorities and Gaps, International Energy Agency, Paris, 2006.
[4] Energy UDo, Hydrogen from Coal Research (2011).
[5] G.T. Rochelle, Science 325 (5948) (2009) 1652–1654.
[6] J. Blamey, E.J. Anthony, J. Wang, P.S. Fennell, Progress in Energy and Combustion Science 36 (2) (2010) 260–279.
[7] L. Dubois, D. Thomas, Chemical Engineering & Technology 33 (10) (2010) 1601–1609.
[8] J. Schell, N. Casas, R. Pini, M. Mazzotti, Adsorption-Journal of the International Adsorption Society 18 (1) (2012) 49–65.
[9] D.D. Papadias, S. Ahmeda, R. Kumar, F. Joseck, International Journal of Hydrogen Energy 34 (15) (2009) 6021–6035.
[10] E.H. Majlan, W.R.W. Daud, S.E. Iyuke, A.B. Mohamad, A.A.H. Kadhum, A.W. Mohammad, M.S. Takriff, N. Bahaman, International Journal of Hydrogen Energy 34 (6) (2009) 2771–2777.
[11] F.V.S. Lopes, C.A. Grande, A.E. Rodrigues, Fuel 93 (1) (2012) 510–523.
[12] A.Y. Abdulla, K. Laney, M. Padilla, S. Sundaresan, J. Benziger, AIChE Journal 57 (2011) 1767–1779.
[13] H.K. Lee, H.Y. Choi, K.H. Choi, J.H. Park, T.H. Lee, Journal of Power Sources 132 (1–2) (2004) 92–98.
[14] S.A. Grigoriev, I.G. Shtatniy, P. Millet, V.I. Porembsky, V.N. Fateev, International Journal of Hydrogen Energy 36 (6) (2011) 4148–4155.
[15] B. Rohland, K. Eberle, R. Strobel, J. Scholta, J. Garche, Electrochimica Acta 43 (24) (1998) 3841–3846.
[16] C. Casati, P. Longhi, L. Zanderighi, F. Bianchi, Journal of Power Sources 180 (1) (2008) 103–113.
[17] K. Onda, K. Ichihara, M. Nagahama, Y. Minamoto, T. Araki, Journal of Power Sources 164 (1) (2007) 1–8.
[18] J. Benziger, J. Nehlsen, Industrial & Engineering Chemistry Research 49 (21) (2010) 11052–11060.
[19] J. Nehlsen, Developing Clean Fuels: Novel Techniques for Desulfurization, Ph.D., Chemical Engineering, Princeton University, Princeton, NJ, 2006.
[20] W.D. An, J.K. Hong, P.N. Pintauro, K. Warner, W. Neff, Journal of the American Oil Chemists' Society 75 (8) (1998) 917–925.
[21] W.D. An, J.K. Hong, P.N. Pintauro, K. Warner, W. Neff, Journal of the American Oil Chemists' Society 76 (2) (1999) 215–222.
[22] J.M. Sedlak, J.F. Austin, A.B. Laconti, International Journal of Hydrogen Energy 6 (1) (1981) 45–51.
[23] B. Ibeh, C. Gardner, M. Ternan, International Journal of Hydrogen Energy 32 (7) (2007) 908–914.
[24] K. Onda, T. Araki, K. Ichihara, M. Nagahama, Journal of Power Sources 188 (1) (2009) 1–7.
[25] T. Suzuki, S.-i. Kawabata, T. Tomita, Present Status of Hydrogen Transport Systems Utilizing Existing Natural Gas Supply Infrastructures in Europe and the USA, Institute of Energy Economics, Japan, 2005.
[26] K. Eberle, B. Rohland, J. Scholta, R. Strobel, Device and Method for Combined Purification and Compression of Hydrogen Containing CO and the Use Thereof in Fuel Cell Assemblies, US Patent 6,361,896, March 26, 2002.
[27] F. Barbir, H. Gorgun, Journal of Applied Electrochemistry 37 (3) (2007) 359–365.
[28] A. Huth, B. Schaar, T. Oekermann, Electrochimica Acta 54 (10) (2009) 2774–2780.
[29] S.S. Kocha, J.D.L. Yang, J.S. Yi, AIChE Journal 52 (5) (2006) 1916–1925.
[30] C.L. Gardner, M. Ternan, Journal of Power Sources 171 (2) (2007) 835–841.
[31] K.A. Perry, G.A. Eisman, B.C. Benicewicz, Journal of Power Sources 177 (2) (2008) 478–484.
[32] S.A. Grigoriev, E.K. Lyutikova, S. Martemianov, V.N. Fateev, International Journal of Hydrogen Energy 32 (17) (2007) 4438–4442.
[33] F. Alcaide, G. Alvarez, P.L. Cabot, O. Miguel, A. Querejeta, International Journal of Hydrogen Energy 35 (20) (2010) 11634–11641.
[34] E. Antolini, Energy & Environmental Science 2 (9) (2009) 915–931.
[35] E. Antolini, S.C. Zignani, S.F. Santos, E.R. Gonzalez, Electrochimica Acta 56 (5) (2011) 2299–2305.
[36] J. Benziger, E. Chia, E. Karnas, J. Moxley, C. Teuscher, I.G. Kevrekidis, AIChE Journal 50 (8) (2004) 1889–1900.
[37] E.S.J. Chia, J.B. Benziger, I.G. Kevrekidis, AIChE Journal 52 (11) (2006) 3902–3910.
[38] G. Sasikumar, J.W. Ihm, H. Ryu, Journal of Power Sources 132 (1–2) (2004) 11–17.
[39] F.A. de Bruijn, D.C. Papageorgopoulos, E.F. Sitters, G.J.M. Janssen, Journal of Power Sources 110 (1) (2002) 117–124.
[40] M.J. Cheah, I.G. Kevrekidis, J. Benziger, Journal of Physical Chemistry B 115 (34) (2011) 10239–10250.
[41] G.J.M. Janssen, Journal of Power Sources 136 (1) (2004) 45–54.
[42] M. Mench, Fuel Cell Engines, Wiley, Hoboken, NJ, 2008.
[43] T. Smolinka, M. Heinen, Y.X. Chen, Z. Jusys, W. Lehnert, R.J. Behm, Electrochimica Acta 50 (25–26) (2005) 5189–5199.
[44] H.A. Gasteiger, S.S. Kocha, B. Sompalli, F.T. Wagner, Applied Catalysis B: Environmental 56 (1–2) (2005) 9–35.
[45] R. Pattabiraman, Applied Catalysis A: General 153 (1–2) (1997) 9–20.